EUROPEAN FUSION DEVELOPMENT AGREEMENT
EFDA
JET

EFDA–JET–PR(06)04

A. Simonetto, C. Sozzi, S. Cirant, S.Garavaglia, A. Bruschi
and JET EFDA contributors

Quasi Optical Interface System for JET's New Microwave Access

Quasi Optical Interface System for JET's New Microwave Access

A. Simonetto, C. Sozzi, S. Cirant, S.Garavaglia, A. Bruschi
and JET-EFDA contributors*

[1]*Istituto di Fisica del Plasma, Associazione EURATOM-ENEA-CNR sulla Fusione,*
via R. Cozzi 53, 20125 Milano, Italy
** See annex of J. Pamela et al, "Overview of JET Results ",*
(Proc. 20th IAEA Fusion Energy Conference, Vilamoura, Portugal (2004)).

Preprint of Paper to be submitted for publication in
Fusion Engineering and Design

ABSTRACT

JET's new Microwave Access system requires a configurable interface to share the transmission lines between the various reflectometric instruments. A confocal quasi optical system made of modular blocks was designed and built for operation in the 60-160GHz range, allowing full configuration and polarization flexibility. This paper deals with the design and test of the instrument.

1. INTRODUCTION AND SPECIFICATIONS

EFDA-JET's new Microwave Access for reflectometry [1] requires that several reflectometers share a common transmission line. A configurable system is required for power- or frequency-splitting among the existing instruments and possible new additions. A reasonable but arbitrary number of instruments can be added. Since transmission lines are made of oversized corrugated circular waveguides, the system must also provide an interface between them and the fundamental waveguide input of the transmitters/receivers. The required bandwidth (in sub-bands) is 60 to 160GHz.

2. SYSTEM DESCRIPTION

The constraints suggested the use of modular blocks (Quasi Optical Boxes, QOB) forming a quasi optical system of mirrors in confocal arrangement, with a magnification factor (focal ratio) chosen for best coupling with fundamental waveguide, to be achieved with a suitable horn. Cost and bandwidth considerations suggested the use of a linear smooth circular horn, accepting the reduced performance with respect to a corrugated feedhorn. Coupling calculations between a fundamental Gaussian beam and the first conical waveguide mode show that commercially available standard gain horns give sub-optimal coupling, irrespective of the magnification factor of the optical system, because their flare angle is too wide. Very large flare angle corrugated horns (that could be used alone, without the last mirror) give best performance only with a focal length very close to the horn size, which is mechanically incompatible with mirrors, because of blockage. Therefore we chose a magnification factor of one *(f2=f1)* in order to use a single mirror type, and designed custom horns with a small flare angle (*5 deg,* limited only by the need to limit the length of the horn).

The system resulting from these design choices, and the ones described below, is shown in fig.1 Horns end with a standard circular waveguide port suited for the lowest frequency required, and commercial (although not always standard) transitions to the proper rectangular waveguide band are fitted to them. Since horns can be replaced easily, should an instrument require lower coupling losses over a narrower band, a suitable corrugated feedhorn can be fitted to a block. The position of the horn aperture with respect to the output focal plane was numerically optimized using physical optics with GRASP [2].

The input corrugated waveguide has an internal diameter of *31.75mm*, and so the HE_{11} is best matched with a fundamental Gaussian mode with a (frequency independent) waist w_O of about *10.2mm* at the waveguide aperture. The Rayleigh distance z_R where the phasefront has a minimum curvature radius ($2*z_R$),

$$z_R = \frac{k w_0^2}{2} \tag{1}$$

is about *120mm* at mid-band (*110Ghz*). Placing the first mirror there, i.e. choosing 120mm for its focal length *f,* the waist w_I in the first (and any odd-rank) focal plane,

$$w_I = \frac{f}{z_R} w_0 \tag{2}$$

varies between $1.83\ w_O = 18.7mm$ at *60 Ghz* and $.69\ w_O = 7.0mm$ at *160Ghz*, whereas on any image plane (even-rank focal plane) the waist is of course the same as that in the corrugated waveguide and is independent on frequency.

The beamwidth w at each mirror varies between *21.3mm* at *60Ghz* and *12.4mm* at *160Ghz,* which dictates a mirror diameter *D* of about *80mm* for minimum *(4*w)* truncation. This leaves room for a grid or other splitting element, whose projected dimension should be about *80mm* to accommodate the beam size at *60GHz.*

The structure should be able, in a future extension, to accommodate Frequency Selective Surfaces (FSS). Usually, FSS have optimum performance for an incident TM polarization, so the minimum impact on the instrument arrangement can be achieved if any pair of mirrors can be made to rotate around the input axis, thus allowing the simplest way of lossless polarization change.

At first, though, only much cheaper wiregrid polarizers will be used, and making them circular and rotatable can simplify usage. The additional truncation loss with respect to rectangular ones (worst case is *2.66 w* for an active grid diameter of *74mm)* has a negligible impact on performance.

As a result of these design choices, a set of modules (Fig.1) was built, each consisting of a mirror and a holder for either a large rectangular splitting element or a smaller rotatable circular one. The mechanical structure takes care of proper aligment and matching of the focal planes at 120mm from each mirror centre. No adjustments are required (nor possible) other than matching the orientation of the polarizer grids with the horns. The interior of the boxes is covered with Eccosorb^{TM} AN72 to provide absorption for any stray radiation.

Each QOB has an input (Quasi Optical) port and two output ones (labelled Reflect and Thru, depending on their orientation with respect to the splitting element). The exploded view of the photograph below shows the components and their labelling.

3. PERFORMANCE CALCULATION

The optical system was designed using standard quasi optics. The horn parameters were optimized computing the coupling between the fundamental Gaussian mode and the first conical waveguide mode [3], then the coupling was computed using GRASP, optimizing the position of the horn at the upper end of the band, where coupling was worse.

The main source of coupling loss is the horn, as expected, because it was designed trading performance with cost and length. The best coupling achievable in theory (infinitely long horn, ie waveguide) is

about *87%*. The finite length of the horn becomes especially important at the highest frequencies, where, on the other side, the optical system is more efficient, as one can see in the plot in fig.3.

The expected insertion loss of the minimum functional unit (two mirrors plus horn) between the input corrugated waveguide, propagating HE_{11} with the proper frequency dependent eigenvalue depending on the corrugation profile, and a circular fundamental waveguide at the end of the horn, is between *1* and *1.5dB*. One can estimate the insertion loss of each pair of mirrors (only due to optical losses) between *0.1* and *0.5dB*, depending on frequency.

The beam shape at the image planes was computed too, and sample results are shown in figure 4. As one can see from the plots, significant distortions from gaussian shape take place only below *–20dB* even in the worst case *(60GHz)*.

Tolerance to misalignment was evaluated in the configuration with two mirrors, one horn and no grids. Coupling variation was evaluated as a function of a small linear (offset) or angular (tilt) displacement of either the second mirror or the horn. Only tilt displacement was evaluated for the input corrugated waveguide. Mirror displacements up to *1mm* cause a variation in transmitted power of only 2%, as shown in fig 5.

Coupling increases at lower frequency because the horn position was optimized at 160GHz, where the beam size can not be matched ideally.

Transverse mirror or horn offsets have a lower impact (*<2%* for *1mm* displacement). A horn (fig.6) or corrugated waveguide tilt up to *0.4 deg* causes a 2% variation in coupling.

4. ELECTROMAGNETIC TESTS

Extensive tests were made with a Vectot Network Analyzer (VNA) [4] in a one port configuration. Each individual QOB was measured injecting power from the horn in the reflect or thru port, with the quasi optical port terminated either with an absorber (Eccosorb^{TM}) or with a flat mirror in the focal plane, to reflect all the power back.

The former configuration allows the direct measurement of the reflection coefficient of a single QOB *(S_{11}* in generalized scattering matrix description). Figure 7 shows a typical result (modulus, in dB). The measurements were made in sub-bands, and all the data are shown together. Between 72 and 75GHz the curve is double valued, because the transition used for WR10 (W-band) to 0.65" circular has a significant reflectivity below the band limit of 75GHz. This effect is not present, of course, in the data taken with the WR15 (V-band) to 0.65" transition. The strong ripple present in the 140-160GHz band is due to an imperfect matching of the WR6 to WR10 transition. Similar results were obtained for all polarizations tested (parallel, perpendicular, and at 45 deg to the reflection plane) and for all the ports (thru or reflect).

Fourier transforming the frequency dependent data allows to localize in time (distance) the points of reflection, and estimate their relative contributions, as shown in figure 8.

The time resolution is limited by the extension of the sub-bands. Since waveguide transitions were different for different sub-bands, joining all the data before transforming was impossible.

Figure 8 is obtained from the 75-110 GHz sub-band. Anyway, the data clearly show distinct echoes for all the discontinuities. The horizontal coordinate is *ct/2*, where the factor 2 accounts for the double delay experienced by the signal propagating towards the load and back to generator.

To have a clear quantitative picture of the relative importance of reflections at various points along the system, the positive and negative time components of the Fourier transformed data were combined, computing the amplitude of the resulting reflection coefficient

$$\left|\rho(t)\right| = \sqrt{\left[\overline{S_{11}}(t)\right]^2 + \left[\overline{S_{11}}(-t)\right]^2} \tag{3}$$

The overbar in (3) denotes the Fourier transformed quantity. The data were then normalized to the largest peak in the Fourier transform of the measurements with a short, and multiplied by the average double path transmittivity (again obtained from measurements with a short), thus obtaining a fair estimate of the reflection coefficient of each discontinuity

$$\left|\rho_{NORM}(t)\right| = \left|\rho(t)\right| \frac{\left\langle \tau^2 \right\rangle}{Max\left[\left|\rho_{SHORT}\right|\right]} \tag{4}$$

The values shown in the plot for all the peaks are very close to the result one would get by simulated time gating on each one individually, i.e. filtering away all the other contributions and inverse Fourier transforming to frequency space.

For measuring the insertion loss (transmittivity) of the QOB, the quasi optical port was terminated with a flat mirror on the focal plane (a short in circuit terms) instead of an absorber. This configuration requires a comment. It was said before that the minimum functional unit is a cascade of two QOB. Since the mirror can be considered a perfect reflector within the precision of these measurements, the configuration we measured was an "unnatural" one, with two QOB (the real one and its reflected image) connected through their quasi optical ports (which is normally prevented by the mechanical structure). This configuration allows to make a meaningful test of each individual QOB and horn antenna. Coupling between Gaussian beams and conical waveguide modes at the antenna is the dominant loss mechanism. Therefore, the addition of a further QOB, in order to measure the coupling between a two-boxes cascade and its mirror image connected through the quasi optical port, is not expected to make much difference, but the measurements would be more difficult because of the larger length of the device under test.

Measuring directly the minimum two port configuration, made of four QOB in two pairs connected with a short corrugated waveguide through their quasi optical ports, was not considered, because it would require a large movement of cables, that would reflect on the precision of the measurements, since our VNA works without a reference mixer.

If the QOB with antenna can be modelled as a two port component, with 1 the measurement port (thru or reflect) and 2 the quasi optical one terminated with the fully reflective load (short), the measured quantity is

$$b_{1,sh} = S_{11} - \frac{S_{12}^2}{1 + S_{22}} \tag{5}$$

since the component is reciprocal. If reflections are small, this is very close to the square of the quantity of interest,S_{12}.

The description as a two port component is not quite obvious, since the quasi optical port of course does support multimode propagation, but one can always choose a linear combination of (gaussian) modes for which the mode mixture excited at the quasi optical port is one of the eigenfunctions, and neglect the other eigenmodes, since they have negligible power, thus restricting the very large generalized scattering matrix to that of a two port. The results are certainly representative of real performance as far as reflections are concerned, whereas the coupling loss between the (unspecified) gaussian mode mixture at the quasi optical port of the QOB and the mixture of hybrid modes in the corrugated waveguide, through a second QOB (the correct working configuration), is not accounted for. Since the corrugated waveguide is significantly oversized, and diffraction losses in the QOB are small, this coupling loss is expected to be very small. Nonetheless, if the mode mixture at the quasi optical port deviated significantly from the one in the corrugated waveguide (e.g. because of an incorrect mode mixture at the circular waveguide port of the horn, that is oversized at the highest frequencies), an additional loss term would appear, unaccounted for by these measurements.

Figure 9 shows the magnitude of the measured transmission coefficient $|S_{12}|$ in a typical case. Even the short configuration we used had a significant length, causing a large path difference between calibration and measurements, that could not be compensated exactly with the cables. It is well known [5] that this path difference can lead to measurement errors if the VNA operates in a swept frequency mode, or, as in our case, the stability of the oscillator was insufficient for the length of the device under test. Allowing more points per sweep would have greatly reduced the problem, but it was not made on all the measurements. When a previous version of the software prevented us to increase the number of points per sweep, we would normally correct the measurements by combining two of them, taken with different lengths of cables [6]. This correction is not applied to the data shown in fig 9. They are therefore a slight overestimate of losses, the correction being about +0.5dB in the lower frequency bands (<110 GHz) and negligible for D band.

Isolation measurements were also made between thru and reflect ports of the same QOB (terminating the quasi optical port with an absorbing load), obtaining coupling values very close to the instrumental noise.

CONCLUSIONS

The eight quasi optical boxes built performed in good agreement with simulations, and the concept of a modular confocal system with no alignment or adjustment appears adequate for use in this diagnostic environment.

REFERENCES

[1]. L. Cupido et al., "New millimeter-wave access for JET reflectometry and ECE", Fusion Engineering and Design **74** (2005) 707–713

[2]. GRASP8, TICRA Engineering Consultants, Copenhagen DK http://www.ticra.com

[3]. Balanis C.A., "Advanced Engineering Electromagnetics", Wiley, New York, 1989

[4]. AB Millimetre, Paris France http://www.abmillimetre.com

[5]. "10 hints for making better network analyzer measurements," Agilent Technol., Palo Alto, CA, Applicat. Note 1291-1B, 2001.

[6]. A.Simonetto, O.D'Arcangelo, L.Figini "Effect of Cable Length in Vector Measurements of Very Long Millimeter-Wave Components", IEEE Transactions on Microwave Theory and Techniques **53**, 12(2005)3731-3734.

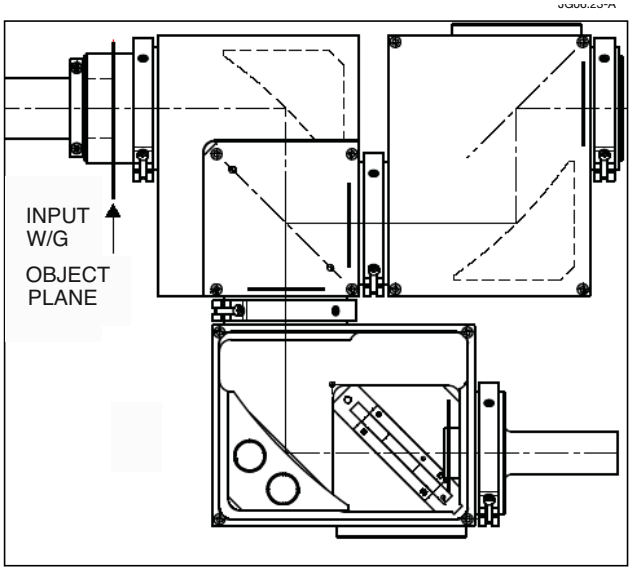

Figure 1: Example of arrangement of the splitting modules. The beam axis is shown. One port (bottom right) terminated with a horn to connect an instrument and up to three (bottom and top right) available for further cascading, depending on grid orientation. The corrugated waveguide input is top left. Each of the blocks can be rotated around the interconnecting flange. The thick black lines show the position of focal planes.

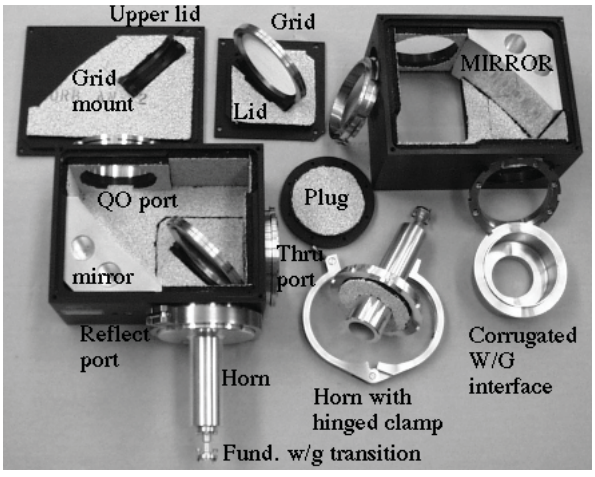

Figure 2: Picture of all the components and their labelling.

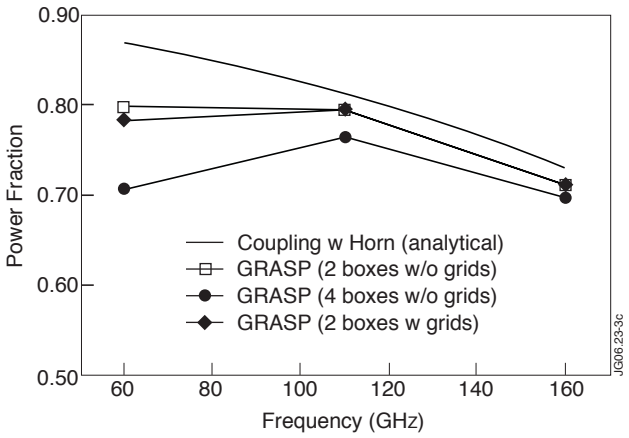

Figure 3: Power coupling between corrugated waveguide and horn antenna in several configurations: 2 and 4 mirrors, no grids (squares and circles), 2 mirrors with grids (diamonds). The analytic calculation of coupling between fundamental GB and horn (continuous line) is shown for comparison.

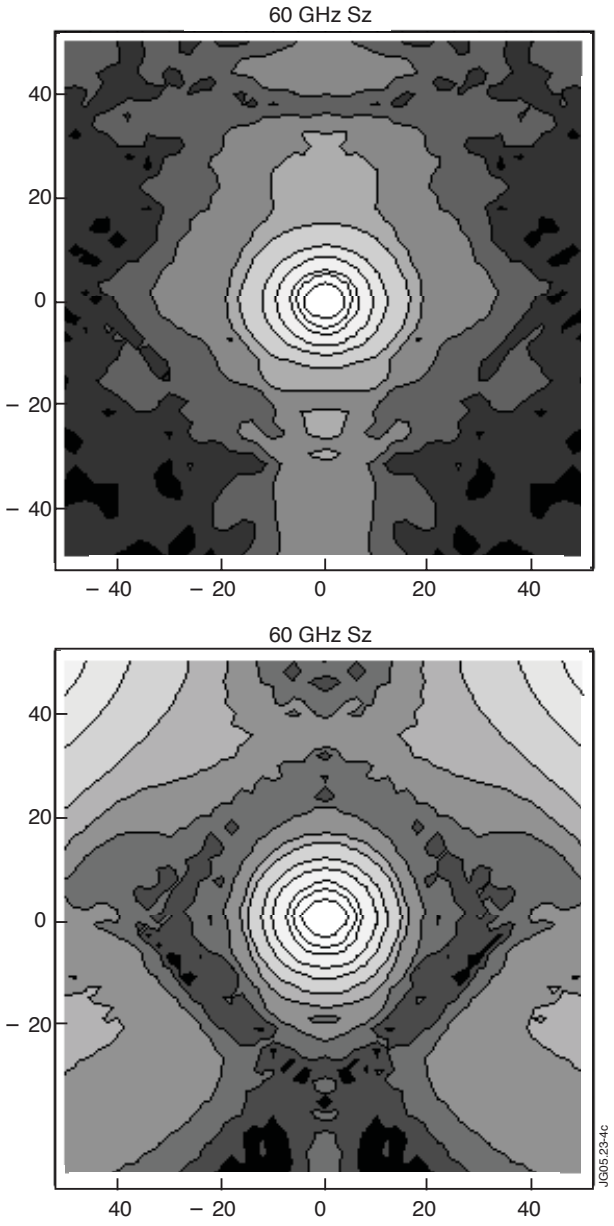

Figure 4: Contour plot of the (computed) component of the Poynting vector parallel to the beam axis at 60 and 160GHz on the output focal plane of a cascade of two QOBs. Contours at –3,–6,–10,–20,–30,–40,–50,–60dB

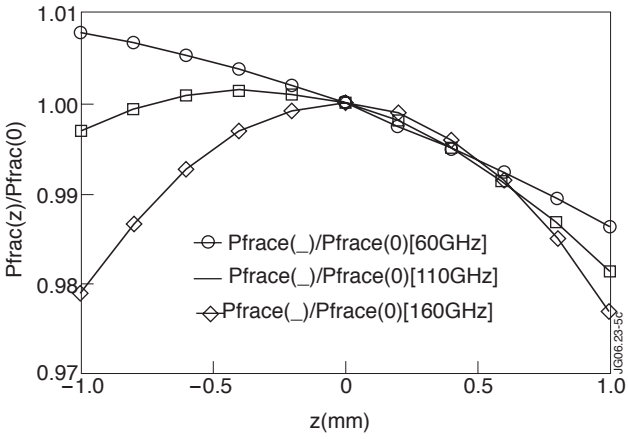

Figure 5: Fractional coupling variation with change in horn-mirror distance. Horn position was optimized at 160GHz, hence the improvement at lower frequency when the horn is moved towards the mirror.

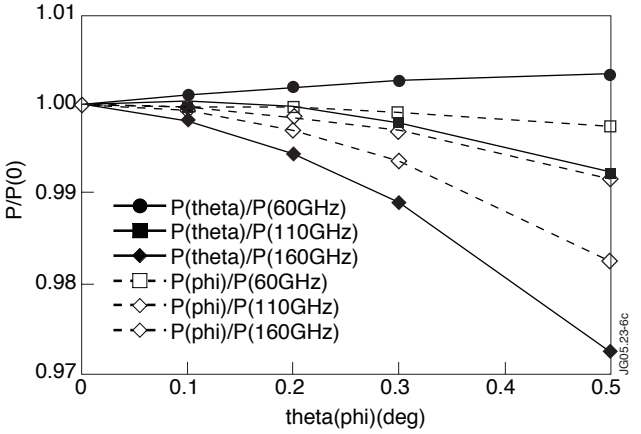

Figure 6: Fractional coupling variation with horn tilt, at several frequencies. Theta is the angle in the last place of reflection, phi is perpendicular to it.

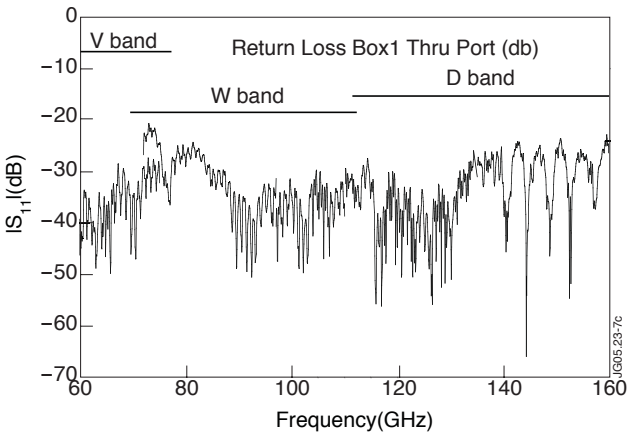

Figure 7: Modulus of the S_{11} scattering parameter. Measurements were taken in sub- bands and curves were plotted together. The double-valued part between 72 and 75GHz is due to the overlap between measurements in V-band and W-band with different transitions. Ripple above 140GHz is due to imperfect mounting of D-W transition

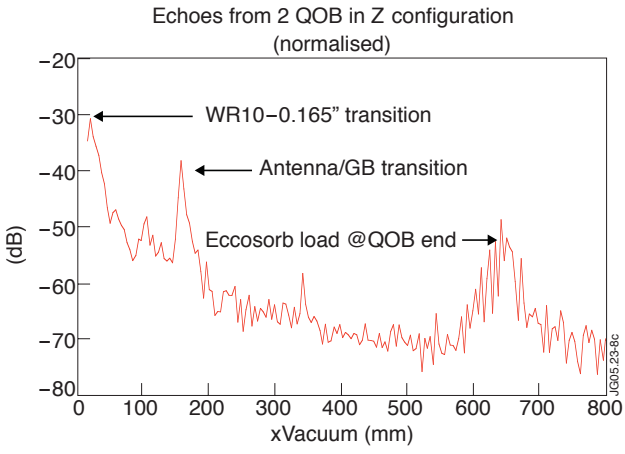

Figure 8: Space localization of reflections from a set of two QOB, from W-band measurements. See text for details on normalization.

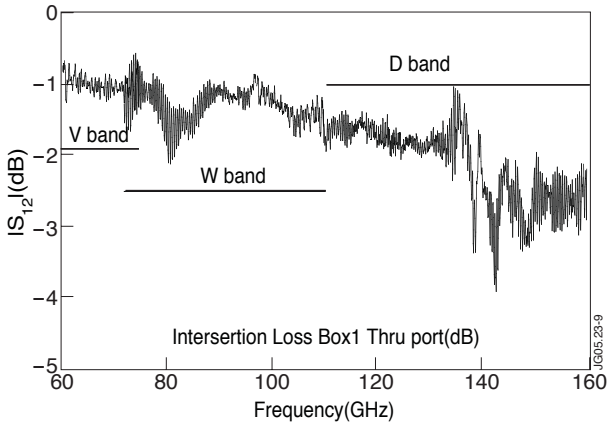

Figure 9: Modulus of the S_{12} scattering parameter. Measurements were taken in sub- bands and curves were plotted together. Ripple above 140GHz due to imperfect mounting of D-W transition. No correction applied for frequency sweep in imbalanced configuration

.

.